Clarification of the Effects of Oxygen Containing Functional Groups on the Pore Filling Behavior of Discharge Deposits in Lithium-Air Battery Cathodes Using Surface-Modified Carbon Gels

Shintaroh Nagaishi[1], Shinichiroh Iwamura[2], Takafumi Ishii[3], and Shin R. Mukai[2*]*

1: Graduate School of Chemical Sciences and Engineering, Hokkaido University, Sapporo 060-6828, Japan

2: Faculty of Engineering, Hokkaido University, Sapporo 060-6828, Japan

3: International Research and Education Center for Element Science, Faculty of Science and Technology, Gunma University, 1-5-1 Tenjin-cho, Kiryu, Gunma, 376-8515, Japan

KEYWORDS

Lithium-air battery, temperature programmed desorption, mesoporous carbon, oxygen-containing functional groups

ABSTRACT

In lithium-air batteries(LABs), controlling the characteristics of the Li_2O_2 deposited during discharging can lead to the reduction of the large overpotential required for charging. The large overpotential is one of the most significant problems which need to be solved to improve the cycle performance of LABs. Here, we focused on the effects of functional groups in the cathode carbon on the characteristics of the Li_2O_2 deposited during discharging and the cathode performance of LABs. In this study, 4 types of carbon gels (CGs) were prepared using different treatment methods to modify their surface properties. The types and amounts of oxygen-containing functional groups (OCFGs) existing within the CGs were clarified along with the number of edge H by a high-sensitivity temperature-programmed desorption (TPD) technique. The results of N_2 adsorption analysis of discharged CGs suggested that, by increasing the number of OCFGs from 0.40 mmol g^{-1} to 1.80 mmol g^{-1} through acid treatment, the ratio of Li_2O_2 deposited within the mesopores of the porous carbon particles can be increased from 1% to 60%. This significant change in the manner of Li_2O_2 deposition led to the reduction of the charging overpotential. Side reactions which are thought to deteriorate cycle performance tended to proceed in CGs having a large number of OCFGs. This negative effect could be reduced by removing carboxyl groups in the CGs through simple heat treatment at 300°C in an inert atmosphere. Our study clarified the critical roles of OCFGs in the cathode during the discharging and charging of LABs. The obtained knowledge can be utilized for the development of a high-performance cathode for LABs.

1 . Introduction

Nonaqueous lithium-air batteries (LABs) are expected to become a promising secondary battery system because they have a higher theoretical energy density than conventional batteries[1]. However, there are still numerous challenging problems to be solved to commercialize this system. Among them, the large overpotentials, which are the difference between thermodynamic potential (2.96 V) and measured potential, are a critical problem which not only leads to a low roundtrip efficiency but also the acceleration of undesired side reactions involving electrolyte decomposition. Nonaqueous LABs are operated through the reactions shown in (1) and (2).

$$Cathode: 2Li^+ + O_2 + 2e^- \leftrightarrow Li_2O_2 \ (1)$$

$$Anode: Li \leftrightarrow Li^+ + e^- \ (2)$$

The discharge reaction terminates when the cathode surface is covered and electrically insulated by low electrically-conductive Li_2O_2 and/or when the supply of O_2 to the cathode is blocked by the deposited Li_2O_2[2 3]. In order to achieve both a large capacity and a high-rate performance, the cathode needs to have a sufficient surface area, a large pore volume to efficiently store Li_2O_2, and also effective diffusion paths for both O_2 and Li^+. Therefore, porous carbon materials are widely used as the cathode material for LABs because of their low density, high inner accessibility and high electrical conductivity. As mesoporous structures can provide both highly accessible surfaces and a large volume of pores for the storage of discharge products, many researchers have used mesoporous carbons as the cathode for LABs in their studies[4-7]. Such studies demonstrated that the discharge capacity depends on the volume and size of mesopores in the porous carbons. Carbon gels (CG) are

one of the candidates for the cathode material with a high capacity because they have a 3-dimensional network of mesopores with a large total volume and narrow size distribution[5, 6, 8].

Both the surface properties and the pore structure of carbon materials significantly influence its performance as a cathode. Belova et al. reported that the increase in the defect density on the surface of a highly ordered pyrolytic graphite cathode promotes the formation of Li_2CO_3 during discharging[9]. In this report, it was explained that Li_2CO_3 was produced through the reaction of the carbon electrode with a lithium superoxide intermediate LiO_2. Thotiyl et al. reported that oxygen-containing functional groups (OCFGs) in carbon materials promote side reactions, through which electrodes and electrolyte are decomposed to form byproducts, such as Li_2CO_3, and that such reactions are accelerated by the high overpotential required for charging[10]. Therefore, highly crystalline and defect-free carbons are preferable to suppress such side reactions. Meanwhile, it has also been reported that the affinity of the cathode carbon to LiO_2 and O_2 affects the characteristics of the deposited Li_2O_2. It has been reported that during discharging, Li_2O_2 with a lower crystallinity tends to be formed on a carbon surface having many OCFGs rather than on a surface with high crystallinity[11]. Li_2O_2 with a low crystallinity can be facilely decomposed in the subsequent charge process at a relatively lower overpotential[12]. DFT calculation has also shown that Li_2O_2 prefers to deposit near defects having functional groups nearby[13]. Therefore, the surface properties of the cathode carbon must be optimized to effectively reduce the overpotential required for charging. In order to regulate the characteristics of the deposited Li_2O_2 and side reactions, the effects of carbon surface properties need to be quantitatively understood.

It is well known that edge sites in carbon materials are chemically and electrochemically more active than their basal planes[14-16]. Therefore, the physical properties and electrode performance of a carbon material are thought to be mainly determined by the properties of the functional groups existing at such edge sites. While a quantitative understanding of functional groups and edge H is important, actual quantification is quite difficult. This is because many types of OCFGs and edge H can hardly be quantified by conventional spectroscopic methods, such as X-ray photoelectron and infrared spectroscopy[17-19]. As an analytical method for OCFGs of carbon materials, temperature-programmed desorption (TPD) is widely known, where gases desorbed at a specific temperature are used to analyze the types and amounts of OCFGs[20-22]. Conventional TPD analysis is conducted by heating a sample under a flow of a carrier gas, such as He and Ar. In this system, the detection sensitivity is not sufficient for analyzing samples having only a small number of OCFGs such as graphite, because the desorption gas from the sample can only be analyzed after being diluted with the carrier gas. Recently, a high-sensitivity TPD technique has been developed, where the sample is heated up to a maximum temperature of 1800℃ under a high vacuum. The desorption gas is directly analyzed by quadrupole mass spectroscopy[23-25]. In this system, the detection sensitivity is very high because the entire amount of the desorption gas can be analyzed. In addition, the total number of edge H can be quantified by heating the sample up to 1800℃, a temperature which is higher than the temperature range in which edge H desorbs as H_2 (800-1500℃)[26]. The high-sensitivity TPD has been used to clarify the relation between carbon edge sites and electrochemical properties of carbons regarding electrochemical degradation in organic electrolytes[27, 28], hydrogen

evolution in an aqueous electrolyte[29], and stability in supercapacitors[30].

Here, we focused on the effects of OCFGs in the cathode carbon on the characteristics of Li_2O_2 deposited during charging and the performance of the carbon as a cathode. Carbon blacks, such as Ketjen black and Super P, are widely used for LAB cathodes. Since the aggregation structure of carbon blacks is mainly determined by van der Waals forces, it can be easily changed by the discharge deposits. Thus, they are thought to be unsuitable for this investigation. In this study, CGs were employed as the porous carbon material for cathodes because they have a highly tunable and stable pore structure, which is practically an aggregation of carbon nanoparticles connected by chemical bonds. Their surfaces can be easily modified because they have numerous edge sites within their structure[6, 31]. CGs were used as a model porous carbon material for the investigation of the effect of heat treatment in the range of 1000-2200℃ on their structure and their cycle performance as a LAB cathode[6]. However, the effects of the OCFGs and edge H within them on their discharge-charge behavior was not investigated in detail because most OCFGs in the CGs were removed by heat treatment above 1000℃, and their surface properties were measured only by a TPD analysis conducted up to a maximum temperature of 1000℃. In this study, the surface properties of CGs were modified by acid treatment and additional heat treatment at 300℃ or 700℃ to vary the type and number of OCFGs in them. Their OCFGs and edge H were precisely analyzed by a high-sensitivity TPD method conducted up to a maximum temperature of 1800℃. The effects of OCFGs in the cathode carbon on the characteristics of Li_2O_2 deposited during discharging, discharge-charge overpotential, and cycle performance were investigated. From the obtained results, we provide quantitative insights into how

OCFGs in CGs affects the pore filling behavior of deposits and cycle performance of CGs as a LAB cathode.

2. Materials and Method

2.1. Materials

Resorcinol (R, 99.0%), formaldehyde (F, 36.0 wt% aqueous solution stabilized by 5–10 wt% methanol), sodium carbonate (C, 99.8%), 2-methyl-2-propanol (99.0%), 1-methyl-2-pyrrolidone (99.0%), nitric acid solution (65 wt%) and acetonitrile (99.8%) were purchased from Fujifilm Wako Pure Chemical Corporation. Tetraethylene glycol dimethyl ether (TEGDME, 99.0%) and CF_3SO_3Li (99.995%) were purchased from Sigma-Aldrich Corporation. Polyvinylidene difluoride (PVDF, KF Polymer #1100) and lithium foil were purchased from KUREHA Corporation and Honjo Metal Corporation, respectively.

2.2. CG preparation

CGs were synthesized according to the literature[5]. First, a mixture of resorcinol (R), distilled water (W), and sodium carbonate(C) was prepared and was thoroughly stirred. After resorcinol and sodium carbonate completely dissolved in the water, formaldehyde (F) was added. R/F, R/W, and R/C ratios in the solution were set to 0.5 mol mol^{-1}, 0.5 g mL^{-1}, and 1000 mol mol^{-1}, respectively. The solution was introduced into a sealable vessel and was first maintained at 30°C for 2 days, then at 60°C for 3 days for gelation and aging. After exchanging the water in the obtained hydrogel with tert-butyl alcohol, the gel was dried in air at 120ºC for 3 days. The dried gel was carbonized at 1000°C for 4 h under a N_2 flow. The

carbonized gel was pulverized by a disk mill (Disk type vibrating mill, Rigaku Co.) for 60 s. The resulting sample will be referred to as p-CG. p-CG was stirred in a nitric acid solution (65%) kept at room temperature for 24 h. The mixture was then filtered under vacuum using a membrane filter with an opening size of 1 μm and washed with distilled water until the pH of the filtrate reached 7. The obtained filtrate was dried at 120℃ for 24 h under a N_2 flow. This sample will be referred to as o-CG. o-CG was heated at 300℃ or 700℃ for 3 h under a N_2 flow. The resulting carbons will be referred to as o-300℃-CG and o-700℃-CG, respectively.

2.3. Characterization

The porous properties of each sample were evaluated through N_2 adsorption experiments conducted at -196°C using an autoadsorber (BELSORP mini, Microtrac Bel Co.). Before experiments, the samples were pretreated at 250°C for 4 h. Pore size distributions were calculated by the Dollimore-Heal (DH) method. The volumes of micropores (V_{micro}; pore diameter smaller than 2 nm) were calculated from the N_2 uptake at $p\ p_0^{-1} = 0.15$. The volumes of mesopores (V_{meso}; pore diameter in 2-50 nm) were calculated by subtracting N_2 uptakes at $P\ P_0^{-1} = 0.15$ from those at $P\ P_0^{-1} = 0.96$. The volumes of macropores (V_{macro}; pore diameter in 50-200 nm) were calculated by subtracting N_2 uptakes at $P\ P_0^{-1} = 0.96$ from those at $P\ P_0^{-1} = 0.99$. The hydrophilicity of each sample was evaluated by H_2O adsorption experiments conducted at 25°C in the relative pressure range of P/P_0 = 0-0.4 using an autoadsorber (BELSORP MAX, Microtrac Bel Co.). The pretreatment conditions of p-CG for H_2O adsorption experiments were at 250°C for 4 h, and those for o-CG and o-300°C-CG

were at 150°C for 4 h. Porous properties of discharged electrodes were also evaluated by N_2 adsorption experiments. The discharged samples were thoroughly washed with acetonitrile to remove the electrolyte and vacuum dried at 150°C for 6 h before N_2 adsorption experiments. Atmospheric exposure of samples during preparation was within a total time of 15 min.

The crystallinity and composition of discharged/charged products on the cathodes were characterized by an X-ray diffractometer (XRD, Ultima IV, Rigaku Co.) with a Cu Kα radiation source operating at 40 kV 50 mA. The 2θ scan range, step width and scan rate were set to 5.0°−80.0°, 0.02° and 5° min^{-1}, respectively. In order to prevent the discharge products from reacting with H_2O or N_2 in the ambient atmosphere, the discharged electrodes were covered with an X-ray permeable cap. Before XRD analysis, the discharged cathodes were thoroughly washed with acetonitrile to remove the residual electrolyte. The structure and morphology of the discharge products formed on the surface of the cathodes were observed using a field emission scanning electron microscope (FE-SEM, JEOL Ltd., JSM-6500F).

2.4. Temperature programmed desorption (TPD) analysis

The OCFGs and edge H existing in each sample were quantified by TPD analysis conducted under vacuum. Before measurements, the samples were vacuum dried at 120°C for 3 h using a vacuum dryer (ETTAS, AVO-250NB, ASONE Co.). After drying, 1-5 mg of the samples was placed in a sample holder made of glassy carbon and set in the vacuum chamber of the TPD apparatus. The chamber was vacuumed by a turbo molecular pump (ULVAC. Inc., UTM-150A) at least overnight to ensure that the pressure of the chamber was below $3.0\times10^{-}$

^{5} Pa prior to analysis. Then the sample was heated by an induction heater (AMBRELL Ltd., EASYHeat 5056 LI) up to 1800℃ at a ramp rate of 10°C min^{-1}. During heating, desorption gases were analyzed by a quadrupole mass spectrometer (QMS, Qulee BGM, ULVAC. Inc., BGM-102). The desorption rates of H_2, CO, CO_2, H_2O, and N_2 were calculated based on calibration curves which were prepared using fragment ions of the gases.

2.5. Fabrication of electrodes

The samples were mixed with a polyvinylidene fluoride (PVDF) binder in N-methyl-2-pyrrolidone (NMP). The weight ratio of sample: PVDF was 19: 1. The obtained slurry was applied to a carbon paper (Toray Industries, Inc., TGP-H-060-4005) at a thickness of 2 mils, using a baker type applicator (TESTER SANGYO CO., SA-201). After drying at 120°C for 15 h under vacuum, the sheet was punched out into circles with a diameter of 16 mm to obtain electrodes, typically coated with 2.0±0.5 mg/sheet of the sample.

2.6. Electrochemical measurements

Coin-type cells are suitable for evaluating practical battery performance. However, it is difficult to disassemble them without damaging the electrode to be analyzed. Therefore, 2 types of test cells were used according to the purpose of the experiment. For cycling tests, 2032-type coin cells (Hohsen Co.) having small holes on the cathode side were used (See Figure S1 in the supporting information). After the sample electrodes were dried under vacuum at 120℃ for 11 h, they were taken into an Ar-filled glove box and test cells were assembled. 100 μL of a mixture of TEGDME and CF_3SO_3Li with a molar ratio of 4: 1, Li

foil (0.2 mm thickness), and a glass fiber filter (Whatman GF/A) were used as the electrolyte, counter electrode, and separator, respectively. The assembled test cell was set in a gas-tight box equipped with tubes. Through the tubes, oxygen was supplied into the box at a flow rate of 10 mL min^{-1}. After a rest period of 10 h in an oxygen atmosphere, the cells were discharged and charged in the range of 2.0-4.4 V at a current density of 50 mA (g-sample) $^{-1}$. During cycling, the charge and discharge capacities were limited to 500 mAh (g-sample)$^{-1}$. Screw-tightened cells which can be disassembled without damaging the electrodes were used for quantitative analysis of the discharged product in the cathode (See Figure S1 in the supporting information). These cells were also assembled in an Ar-filled glove box. Measurements were conducted through the same procedure using the same components as for the coin-type cells.

3. Results and discussion

3.1. Pore structure of CGs

N_2 adsorption isotherms of the CGs and pore size distributions derived from the isotherms are shown in Figures 1 and 2, respectively. The obtained isotherms show N_2 uptakes at an extremely low relative pressure ($P\ P_0^{-1}$) and the $P\ P_0^{-1}$ of 0.9 which indicate that the CGs have micro/mesopores. BET surface areas (S_{BET}), micropore volumes (V_{micro}), mesopore volumes (V_{meso}), and macropore volumes (V_{macro}) calculated from the isotherms are summarized in Table1. S_{BET}, V_{micro}, and V_{meso} of p-CG are almost equal to those of o-CG, showing that oxidation hardly affected the pore structure of CGs. On the other hand, heat treatment after oxidation affected S_{BET} and V_{micro} of the CGs, both of which increased with the increase in the heat treatment temperature. The differences in micropore structure are

thought not to affect the results of electrochemical measurements, as micropores hardly affect the discharge capacity of LABs[32]. While V_{meso} of o-300°C-CG and o-700°C-CG were slightly larger than those of p-CG and o-CG, their mesopore size distributions were basically the same (Figure 2). The increase in V_{meso} is not due to the introduction of mesopores but due to the decrease in the weight of CG particles caused by heat treatment. Therefore, the influences of the difference in pore structures on the results of electrochemical measurements are thought not to be significant.

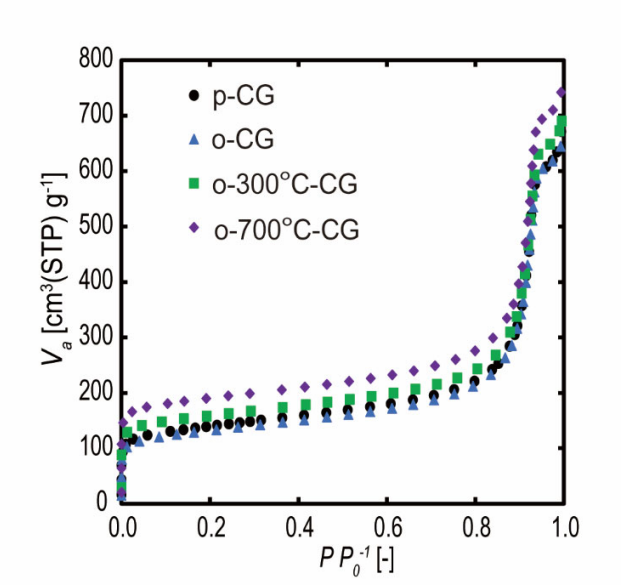

Figure 1 N_2 adsorption isotherms of the surface modified CGs (77 K).

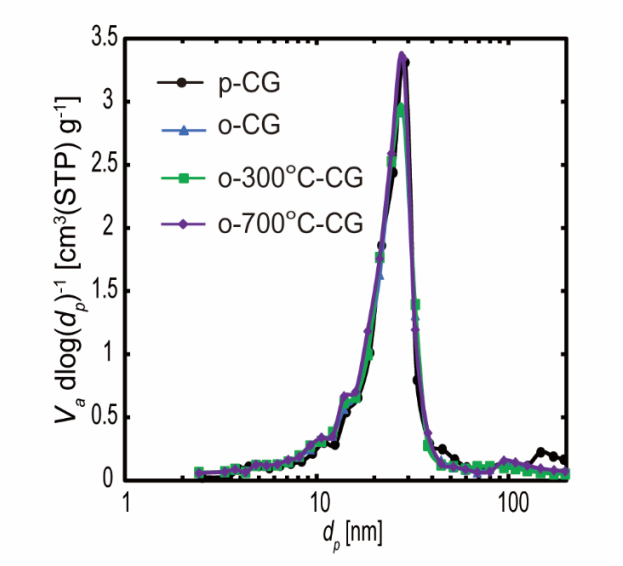

Figure 2 Pore size distributions of the surface modified CGs determined by the DH method.

Table 1 Textural properties of the CGs characterized by N_2 adsorption experiments.

	S_{BET}[a] [cm^3 g^{-1}]	V_{micro}[b] [cm^3 g^{-1}]	V_{meso}[c] [cm^3 g^{-1}]	V_{macro}[d] [cm^3 g^{-1}]	d_p[e] [nm]	$X_{0.15}$[f]
p-CG	473	0.21	0.73	0.07	29	0.03
o-CG	478	0.20	0.75	0.05	29	0.15
o-300°C-CG	568	0.24	0.76	0.05	29	0.08
o-700°C-CG	722	0.29	0.80	0.05	29	0.03

a Determined from the data at $p\ p_0^{-1}$ = 0.1–0.2.

b Calculated from the N_2 uptake at $p\ p_0^{-1} = 0.15$.

c Calculated from the difference between N_2 uptakes at $p\ p_0^{-1} = 0.96$ and $p\ p_0^{-1} = 0.15$

d Calculated from the difference between N_2 uptakes at $p\ p_0^{-1} = 0.99$ and $p\ p_0^{-1} = 0.96$

e Peek top diameter d_p calculated by applying the DH method to the adsorption isotherms.

f $X_{0.15}$ was calculated by the H_2O uptake at $p\ p_0^{-1} = 0.15$ divided by N_2 uptake at $p\ p_0^{-1} = 0.15$.

3.2. Surface characteristics of CGs

The hydrophilicity of the surface-modified CGs was evaluated by H_2O adsorption experiments. The H_2O adsorption isotherms of the samples are shown in Figure 3. Porous carbons adsorb H_2O atoms through micropore filling typically at $P\ P_0^{-1}$ = 0.5-0.75 and through mesopore filling typically at $P\ P_0^{-1} > 0.75$.[33]. To compare the amounts of surface adsorption without the influence of their pore structure, we employed the adsorption amounts at $P\ P_0^{-1}$ =0.15 to evaluate hydrophilicity. $X_{0.15}$ which is the ratio between the H_2O and N_2 uptake values of the sample both measured at $P\ P_0^{-1} = 0.15$ were calculated and the results are listed in Table 1. The $X_{0.15}$ value of o-CG was larger than that of p-CG, meaning that the surfaces of p-CG became more hydrophilic by acid treatment. On the other hand, heat treatment after oxidation led to a decrease in the $X_{0.15}$ value which became more significant when the heat treatment temperature was increased. These results suggest that some OCFGs of o-CG were removed during heat treatment.

OCFGs and edge H of CGs were analyzed by TPD measurements. Figure 4 shows the TPD spectra of the obtained samples. The total amounts of H_2, H_2O, N_2, CO_2, and CO which

desorbed during TPD analysis are summarized in Table2. Among these gases, CO and CO_2 correspond to the desorption from OCFGs. The total amount of CO and CO_2 which desorbed from p-CG was 0.46 mmol $g^{-1,}$ and that from o-CG was 2.0 mmol g^{-1}, indicating that a significant number of OCFGs was introduced by acid treatment. The corresponding amounts of o-300°C-CG and o-700°C-CG were 1.62 mmol g^{-1} and 0.79 mmol g^{-1}, respectively. The TPD spectra of these samples show that desorption of CO and CO_2 starts when the temperature exceeds the temperature of heat treatment after oxidation. These results suggest that OCFGs detach from the samples according to their thermal stability, and the type and number of OCFGs which remain after heat treatment can be controlled by adjusting the maximum treatment temperature.

The total amount of N_2 which desorbed from p-CG was 0.02 mmol g^{-1}, indicating a small amount of N atoms were incorporated into the sample during carbonization under a N_2 flow. The total amount of N_2 in o-CG was 0.18 mmol g^{-1} which was larger than that of p-CG, indicating that the N-containing functional groups were formed during HNO_3 treatment. Those of o-300°C-CG and o-700°C-CG were 0.12 mmol g^{-1} and 0.11 mmol g^{-1}, respectively. Like OCFGs, N-containing functional groups also detach from the samples according to their thermal stability.

In order to estimate the number of each type of OCFG, peak separation of the TPD spectra of CO and CO_2 was conducted (See Figure S2 supporting info.). The desorption temperature and full width at half maximum (FWHM) of the OCFGs were determined according to the literature[20, 23 24]. Table 3 shows the number of each type of OCFG in CG samples determined from peak separation. p-CG had several types of OCFGs, whose distribution was similar to

that of o-CG although there is a large difference in the number of them. The number of carboxyl groups in o-CG (0.227 mmol g^{-1}) was significantly larger than that in o-300°C-CG (0.004 mmol g^{-1}); the amounts of other groups, such as carbonyl, phenol/ether, lactone, and anhydride, were similar. This indicates that heat treatment at 300°C selectively removed carboxyl groups. Similarly, o-700°C-CG hardly contains OCFGs, which can be thermally decomposed at temperatures below 700°C, such as carboxylic, anhydride, and lactone.

The H_2 desorption spectra of all samples showed a peak in the range of 850-1600°C, which corresponds to the desorption from edge H. However, the number calculated from the entire amount of H_2 desorbed in this range leads to an overestimation of edge H because carboxylic and phenol groups also contribute to H_2 desorption in this temperature range[23]. Carboxylic groups decompose and generate CO_2 and edge H at around 300℃. Similarly, phenol groups decompose to CO and edge H at 600-900℃. However, separating the peaks corresponding to phenol and ether groups from a TPD spectra is difficult because both groups decompose and generate CO in the same temperature range[23]. Therefore, maximum and minimum numbers of edge H were respectively calculated using the following equations which assume that all of the CO generated in this temperature range were only from either ether groups or from phenol groups.

$$N_H(\max) = 2 \times N_{H2} - N_C \quad \text{(EQ1)}$$

$$N_H(\min) = 2 \times N_{H2} - N_C - N_P \quad \text{(EQ2)}$$

where N_H is the number of edge H, N_{H2} is the total amount of H_2 which desorbs at temperatures above 850℃, N_C is the number of carboxylic groups and N_P is the number of phenol/Ether groups, respectively. Furthermore, the total number of sites of each sample to

which OCFGs or edge H are attached were calculated by eq3.

$$N_{Edge} = N_H + N_C + N_P + 2 \times N_L + 2 \times N_A + N_{Ca} \quad \text{(EQ3)}$$

where N_{Edge} is the total number of sites, N_L is the number of lactone groups, N_A is the number of anhydride groups and N_{Ca} is the number of carbonyl groups, respectively.

As shown in Figure 5, while the number of OCFGs and edge H significantly changed by acid treatment, N_{Edge} did not change so much. These results indicate that the oxidation process replaced edge H with OCFGs. In addition, while the number of OCFGs and edge H in o-CG, o-300°C-CG, o-700°C-CG differed, their N_{Edge} were not largely different. These results indicate that the heat treatment destroyed some OCFGs and then generated edge H. Thus, these samples are thought to be suitable for the investigation of how OCFGs of porous carbon affect the cathode performance of LAB.

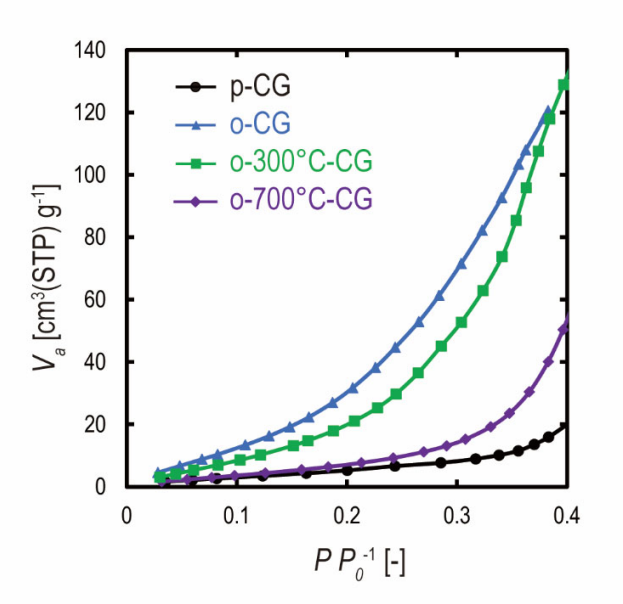

Figure 3 H_2O adsorption isotherms of surface-modified CGs (298 K).

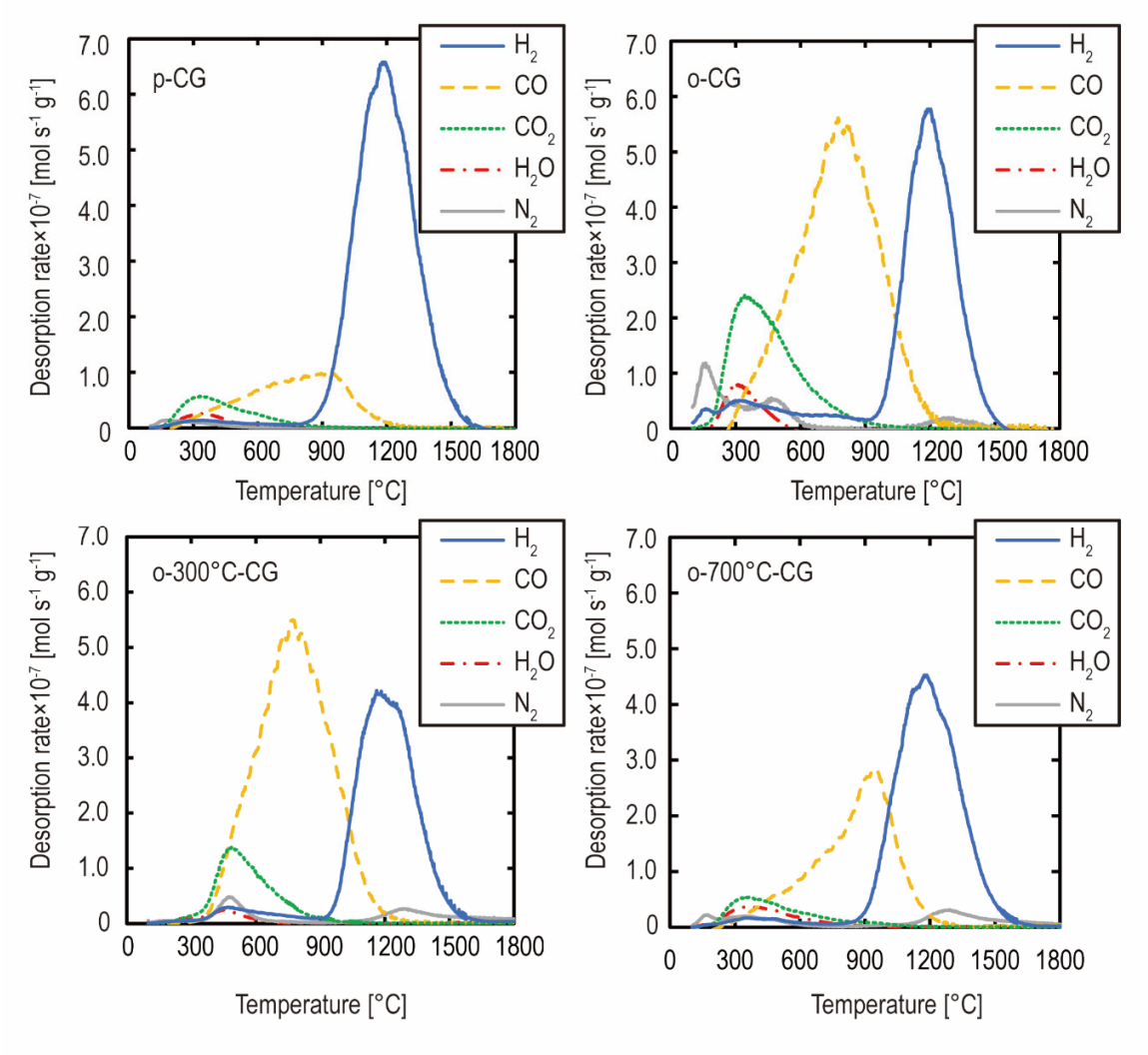

Figure 4 TPD spectra of surface-modified CGs.

Table 2 Total amounts of gases desorbed from CGs during TPD analysis.

	H_2 [mmol g^{-1}]	CO [mmol g^{-1}]	CO_2 [mmol g^{-1}]	N_2 [mmol g^{-1}]	H_2O [mmol g^{-1}]
p-CG	1.34	0.34	0.12	0.02	0.04
o-CG	1.08	1.52	0.50	0.18	0.09
o-300°C-CG	0.89	1.38	0.24	0.12	0.04
o-700°C-CG	0.98	0.66	0.13	0.11	0.09

Table 3 The number of OCFGs of surface modified CGs determined from peak separation.

	Carboxylic [mmol g^{-1}]	Anhydride [mmol g^{-1}]	Lactone [mmol g^{-1}]	Phenol/Ether [mmol g^{-1}]	Carbonyl [mmol g^{-1}]
CG	0.063	0.039	0.020	0.128	0.145
Ox-CG	0.227	0.208	0.065	0.711	0.589
Ox-300°C-CG	0.004	0.154	0.077	0.727	0.515
Ox-700°C-CG	0.057	0.031	0.028	0.193	0.402

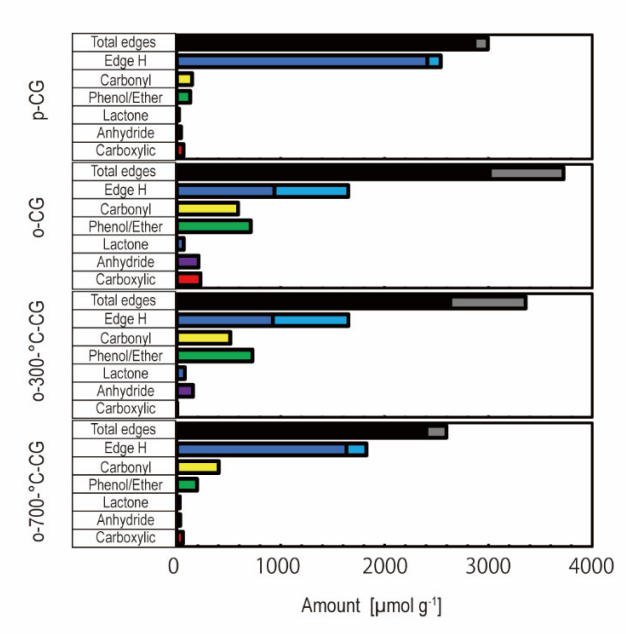

Figure 5 The number of sites in surface-modified CGs to which certain OCFGs or edge H are attached obtained from TPD analysis. The gray and light blue bars present the upper and under limit of total sites and edge H, respectively.

3.3. Influence of surface properties of CGs on overpotential

Discharge-charge measurements of the CGs were conducted using coin-type cells. When the cells were discharged without capacity limitation, the cells worked only for a limited number of cycles. Therefore, for the evaluation of their cycle performance, the discharge capacity was limited to 500 mAh g^{-1}. The volume of the Li_2O_2 deposited at this discharge capacity is 0.186 cm^3 g^{-1} calculated using the density of Li_2O_2 (2.3 g cm^{-3}), which corresponds to 23-25% of the mesopore volume of the CGs. Figure 6 shows the obtained discharge-charge curves. The curves of all the CGs show similar discharge overpotentials. This suggests that the number of OCFGs hardly affected the activity of the oxygen reduction

reaction. On the other hand, the charge overpotential was quite different among the samples until the charge capacity reached 300 mAh g^{-1}; The overpotential decreased with the increase in the number of OCFGs.

During discharging, Li_2O_2 deposits by electrochemical reduction on the carbon surface (surface-route) or through solution-mediated chemical disproportionation (solution-route)[12, 34], which can be formulated as follows.

$$O_2 + e^- \rightarrow O_2^- \quad (3)$$

$$Li^+ + O_2^- \rightarrow LiO_2 \quad (4)$$

$$2LiO_2(sol) \rightarrow Li_2O_2 + O_2 \quad (5)$$

In the surface-route, low crystalline Li_2O_2 deposits in the form of a film. In the solution-route, toroidal-shaped and high-crystalline Li_2O_2 deposits in the electrolyte. Li_2O_2 formed through the solution-route generally requires a higher overpotential to be charged (decomposed) than that formed through the surface-route. The crystallinity and morphology of Li_2O_2 deposited on the cathodes discharged at 500 mAh g^{-1} were investigated by XRD analysis and SEM observation. The XRD patterns shown in Figure 7 had peaks at 2θ = 32.9°, 35.2°and 58.7°, which can be assigned to (100), (101), and (110) of Li_2O_2, respectively, while other crystalline materials such as Li_2CO_3 and LiOH, were not observed. Peaks at 54º of the cathode prior to discharging are identified as the (004) reflections of carbon originating from the carbon paper[5]. The XRD pattern including the data in the range of 10 to 30º shown in Figure S3 of the supporting information, indicates that the structure of carbon was not changed after discharging. From these peaks, the crystallite size of Li_2O_2 was calculated according to the Scherrer's formula and the results are summarized in Table 4. These results

suggest that crystalline Li_2O_2 with a particle size larger than 60 nm was deposited on all the CG cathodes through the solution-route. Since such large particles cannot deposit inside the pores of the CGs, the Li_2O_2 particles should exist on the outer surface of the CG particles. From the SEM images shown in Figure 8, toroidal-shaped Li_2O_2 particles, which is a typical structure of Li_2O_2 formed via the solution-route, with a diameter of around 1 μm were clearly observed on the outer surface of each sample. Amorphous Li_2O_2 films deposited through the surface-route were not observed. As each sample included Li_2O_2 which could be decomposed at a relatively lower overpotential, it can be expected that part of the Li_2O_2 was deposited inside the pores of the CGs through the surface-route.

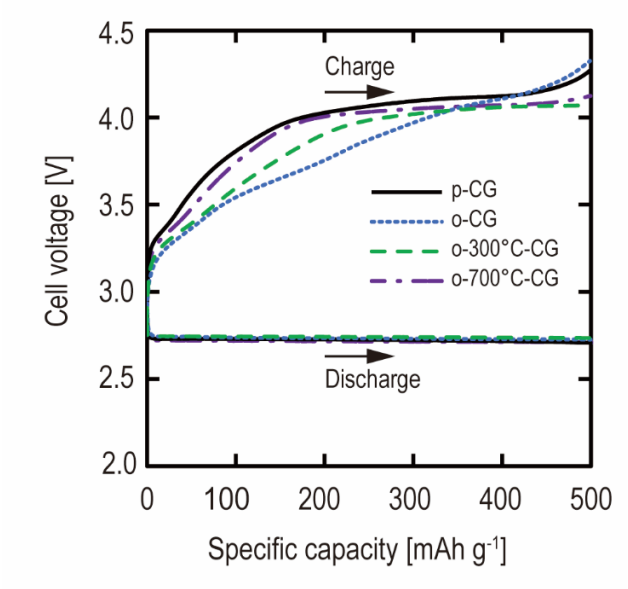

Figure 6 Discharge-charge curves of surface-modified CGs. (Current density: 50 mA g^{-1}, discharge-charge capacity limitation: 500 mAh g^{-1}) The measurements were conducted using coin-type cells.

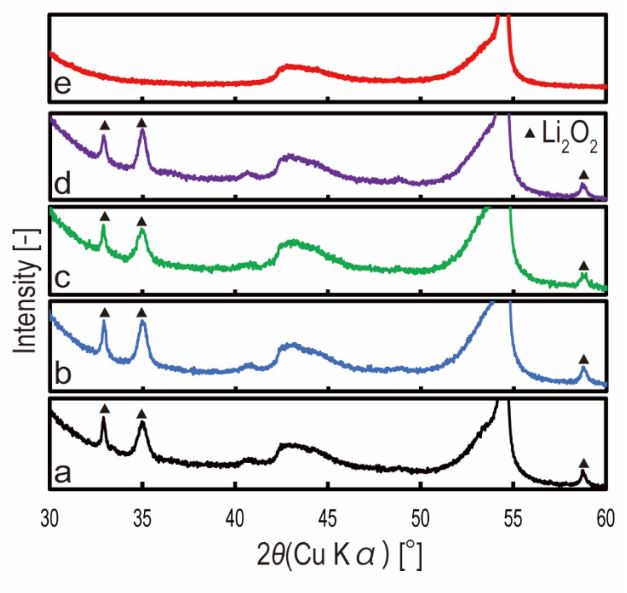

Figure 7 XRD patterns of the electrodes of (a)p-CG, (b)o-CG,(c)o-300°C-CG, and (d)o-700°C-CG discharged for 500 mAh $g^{-1}$and (e)p-CG before discharge.

Table 4 Crystallite size of Li_2O_2 deposited on CGs discharged for 500 mAh g^{-1}. The sizes were estimated from the XRD patterns by Scherrer's formula.

	Crystallite size (100) [nm]	Crystallite size (101) [nm]
p-CG	63	26
o-CG	59	26
o-300°C-CG	67	24

o-700℃-CG	58	34

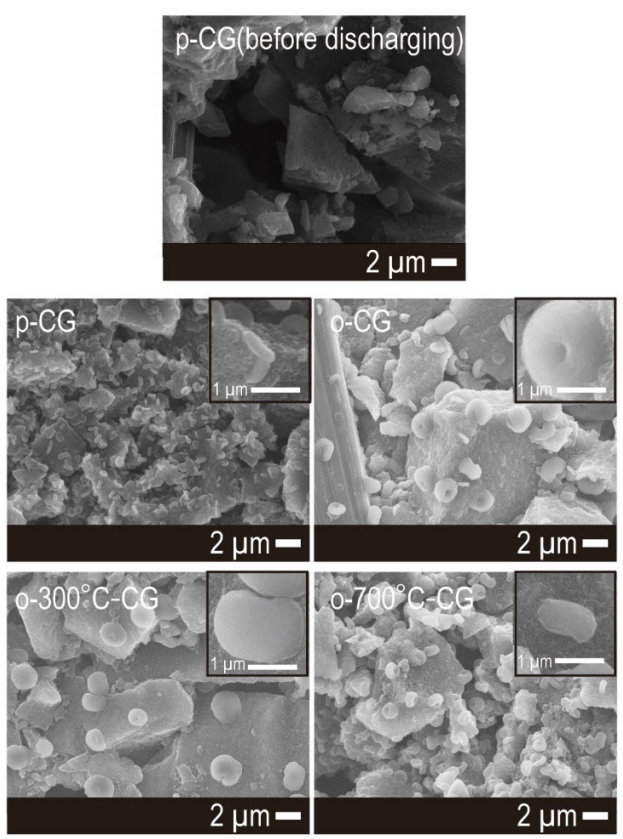

Figure 8 FE-SEM images of the CG cathodes before discharging, and after discharged for 500 mAh g^{-1}

3.4. Pore filling behavior of Li_2O_2

To estimate the ratio between the volume of Li_2O_2 deposited within the pores and that deposited on the outer surface of the CG particles, the pore structure of CG cathodes prior to discharging and after discharging for 500 mAh g^{-1} was analyzed by N_2 adsorption

experiments. Cathodes which were not discharged were soaked in the electrolyte, washed with acetonitrile, and dried. This washing procedure was also adopted for the discharged cathodes before N_2 adsorption analysis. Figures 9 and 10 show N_2 adsorption isotherms of the cathodes and pore size distributions derived from the isotherms, respectively. S_{BET}, V_{micro}, V_{meso}, and V_{macro} calculated from the isotherms are summarized in Table5. Table 1 and Table 5 show the data of the samples prior to and after cathode preparation, respectively. Although the CGs originally had a micropore volume of 0.20-0.29 $cm^3\ g^{-1}$ (Table 1), it decreased to 0.07-0.08 $cm^3\ g^{-1}$ (Table 5) when combined into the cathode and soaked with the electrolyte and washed. The decreases in V_{micro} are thought to be caused by the binder and electrolyte, as previously reported[5, 35]. The micropore volumes remained almost unchanged after discharging, indicating that Li_2O_2 was not deposited in the micropores. While the mesopore volumes hardly changed by soaking in the electrolyte followed by washing, they were significantly reduced after discharging which means that the mesopores were filled with discharge deposits. It was also found that the amount of reduction in mesopore volume varied according to the CG sample. While the estimated total volume of Li_2O_2 deposited at the discharge capacity of 500 mAh g^{-1} is 0.186 $cm^3\ g^{-1}$, the reduction in mesopore volume of each sample was smaller than this volume. Thus, part of Li_2O_2 should have deposited outside the mesopores. The peak position of the pore size distribution shifted to a smaller value after the cathode was discharged for 500 mAh g^{-1}, indicating that the deposits filled the mesopores and the pores became narrower.

The macropore volumes were calculated by subtracting N_2 uptakes at $P\ P_0^{-1} = 0.96$ from those at $P\ P_0^{-1} = 0.99$; therefore, this volume corresponds to the volume of macropores with

a diameter in the range of 50-200 nm. The amount of N_2 adsorption in the isotherms of all of the CGs rapidly increased in the relative pressure range of 0.8-0.96 and then moderately increased in the range of 0.96-0.99. These trends suggest the presence of two types of porous structures: pores in the particles and inter-particle voids. When CGs with different particle sizes were analyzed by N_2 adsorption experiments, the volume of N_2 adsorbed in the relative pressure range of 0.96-0.99 increased with the decrease in particle size of the CG (See Figure S5 in the supporting information), indicating that the inter-particle voids can be analyzed through N_2 adsorption experiments. As the CG powders originally had macropores with a volume of 0.05-0.07 $cm^3\ g^{-1}$ (Table 1), these volumes slightly increased to 0.06-0.08 $cm^3\ g^{-1}$ (Table 5) when the powders were combined into the cathodes and soaked in the electrolyte, indicating that the process to prepare electrodes formed voids corresponding to macropores. In addition, the macropore volume further increased to 0.08-0.12 $cm^3\ g^{-1}$ after discharging for 500 mAh g^{-1}, suggesting that Li_2O_2 which deposited outside the particles formed voids corresponding to macropores.

In order to evaluate the utilization efficiency of mesopores in CGs for Li_2O_2 deposition, the volumes of Li_2O_2 deposited inside the mesopores of the CGs were compared. Assuming that the reduction in the volume of mesopores caused by discharging is equal to the volume of Li_2O_2 deposited in the mesopores, the percentages of the volume of Li_2O_2 deposited in the mesopores based on the total volume of Li_2O_2 deposited on the cathodes were calculated. The results are shown in Figure 11. The percentages of p-CG and o-700°C-CG cathodes were only 1% and 26%, respectively, indicating that most of the Li_2O_2 was deposited outside the mesopores. On the other hand, the percentages of o-CG and o-300°C-CG cathodes were 60%

and 64%, respectively, indicating that Li_2O_2 was mainly deposited inside the mesopores. The S_{BET} of p-CG and o-700℃-CG cathodes increased by discharging, while that of o-CG and o-300℃-CG cathodes decreased. This may be because the Li_2O_2 deposited outside the CG particles contributed to the increase in surface area, further supporting that the volume of Li_2O_2 deposited inside the CG particles was low. The size of the Li_2O_2 particles calculated from the increases in S_{BET} of p-CG and o-700℃-CG were about 90 nm and 40 nm, respectively, which are of the same order as the crystallite size determined from the XRD peaks using Scherrer's formula. The size of Li_2O_2 particles deposited on the outer surface of o-CG and o-300℃-CG cathodes is larger, and the number of them is smaller than those deposited on p-CG and o-700℃-CG (Figure 8). As explained in 3.2, the number of OCFGs in o-CG and o-300°C-CG is larger than those in p-CG and o-700°C-CG. These results suggest that OCFGs in o-CG and o-300°C-CG cathodes promote the formation of Li_2O_2 within the particle and therefore the relative amount of Li_2O_2 deposited outside the CG particles became smaller. In addition, the results of p-CG indicate that edge H does not promote the formation of Li_2O_2 within the particle. The results of o-CG and o-300°C-CG revealed that carboxyl groups do not have a significant effect on the formation of Li_2O_2 inside mesopores. Also, it is concluded from the results of o-300°C-CG and o-700°C-CG that the effective functional groups on Li_2O_2 deposition inside mesopores are either anhydride, lactone, or phenol/ether. It is assumed that as the Li_2O_2 deposited inside mesopores was smaller than that deposited outside the particle, the small Li_2O_2 particles had sufficient electrically conductive paths connected to them, and the overpotential required for charging became lower.

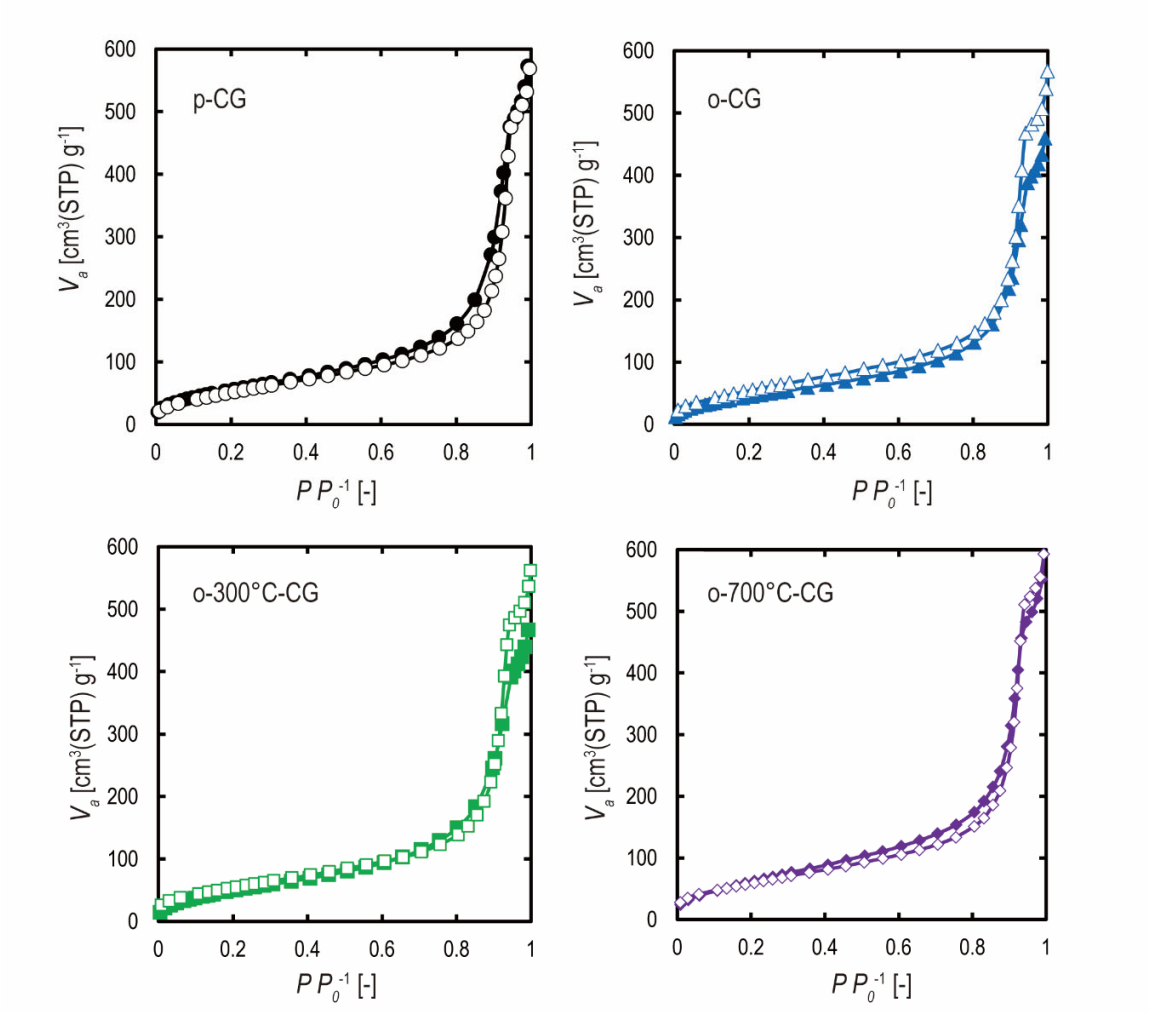

Figure 9 N_2 adsorption isotherms of the surface-modified CGs cathodes (empty symbols) prior to and (filled symbols) after discharging for 500 mAh g^{-1}.

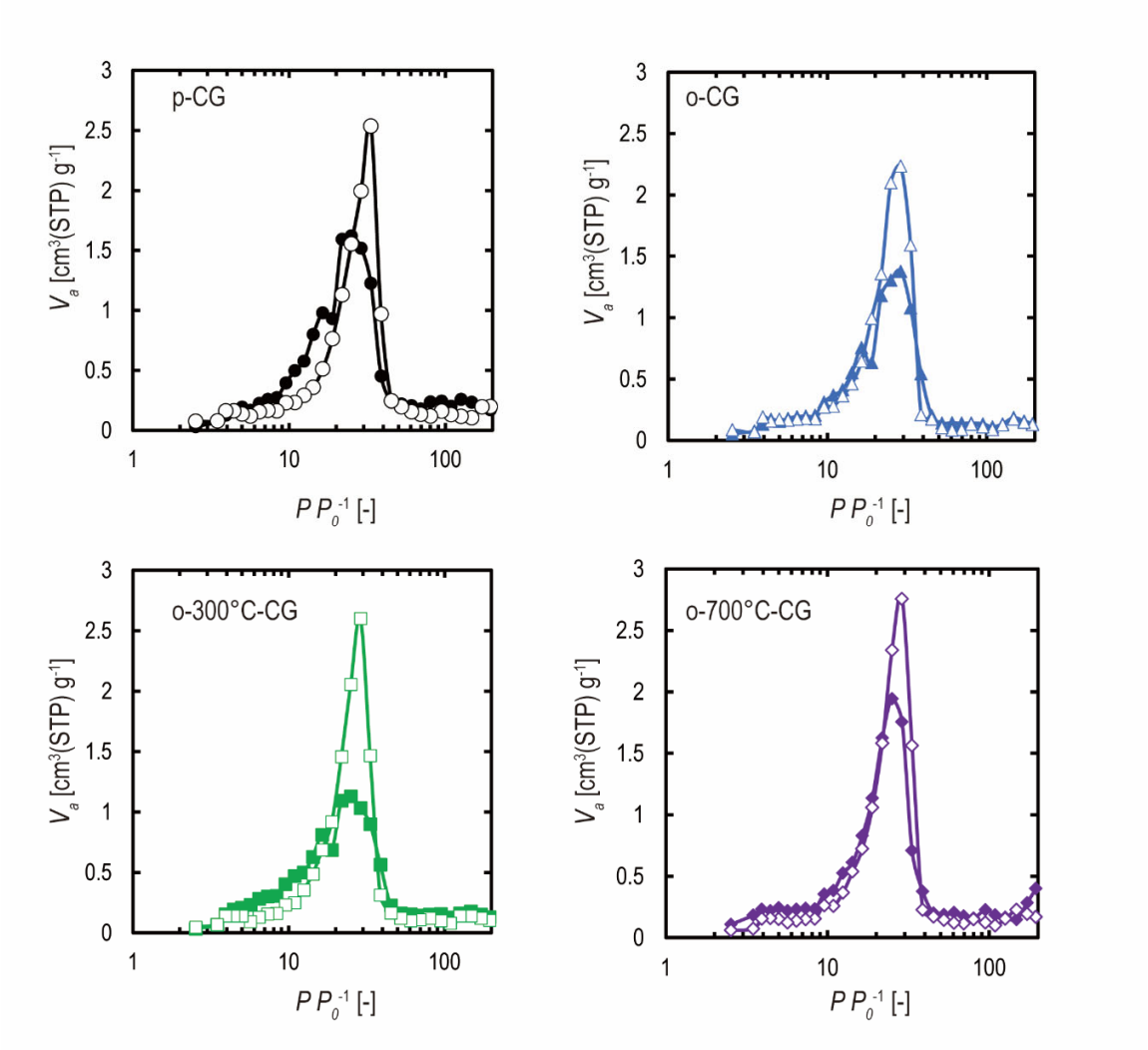

Figure 10 Pore size distributions determined by the DH method of the surface-modified CG cathodes (empty symbols) prior to and (filled symbols) after discharging for 500 mAh g^{-1}.

Table 5 Porous properties of CG cathodes prior to and after discharging for 500 mAh g^{-1}

sample	State	S_{BET} [m^2 g^{-1}]	V_{micro} [cm^3 g^{-1}]	V_{meso} [cm^3 g^{-1}]	V_{macro} [cm^3 g^{-1}]
p-CG	Prior to discharging	199	0.07	0.69	0.08
o-CG		212	0.07	0.67	0.06
o-300°C-CG		203	0.08	0.68	0.06
o-700°C-CG		219	0.08	0.73	0.08
p-CG	After discharging for 500 mAh g^{-1}	211	0.08	0.69	0.12
o-CG		173	0.06	0.56	0.08
o-300°C-CG		190	0.07	0.56	0.08
o-700°C-CG		240	0.08	0.68	0.11

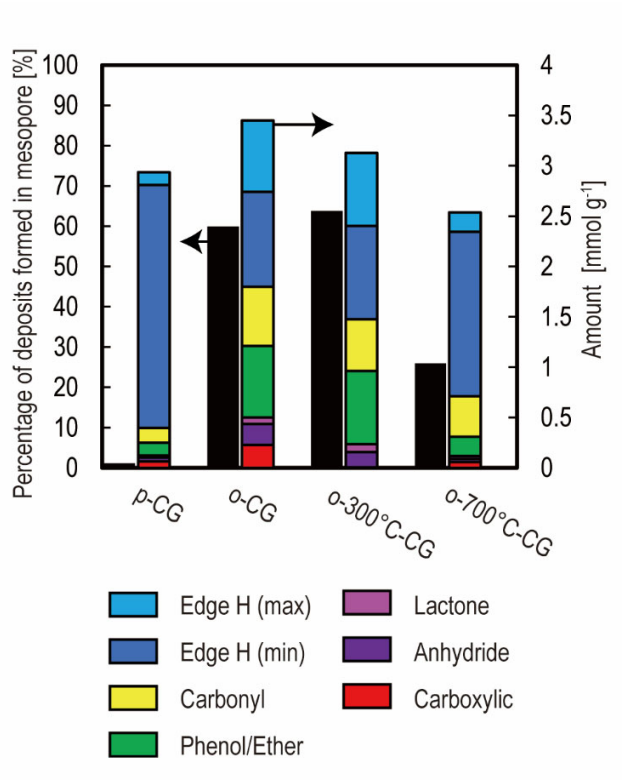

Figure11 The relationship between the percentage of deposits formed in mesopores and the number of OCFGs and edge H in the surface-modified CG cathodes. The percentage of deposits formed in mesopores was calculated by (V_{meso} prior to discharge – V_{meso} after discharging for 500 mAh g^{-1}) divided by the volume (0.186 cm^3 g^{-1}) corresponding to Li_2O_2 deposited at the discharge capacity of 500 mAh g^{-1}.

3.5. Influences of the surface properties on Cycle performance

Discharge-charge cycle tests were conducted using coin-type cells to investigate how the surface properties of CGs affects cycle performance. Matsuda et al. reported that practical LAB cells with energy densities of 414-610 Wh kg^{-1} can be assembled[36]. Since the weight of the carbon cathode was 5 mg cm^{-2}, the current density (0.4 mA cm^{-2}) and capacity limit (6

mAh cm^{-2}) they set correspond to 80 mA g^{-1} and 1200 mAh g^{-1}, respectively. Thus, the employed values of 50 mA g^{-1} and 500 mAh g^{-1} is sufficiently high for practical uses. Figure 12 shows how the charge and discharge capacities of the CG cathodes changes during cycling. The charge and discharge curves of the cycle tests are shown in Figure S7 in the supporting information. In all samples, the overpotential required for charging increased as the charge-discharge cycle was repeated. The charge capacity of p-CG started to fade at the 5th cycle, while its discharge capacity was maintained at the set value (500 mAh g^{-1}) for 20 cycles. This indicates that the deposits formed during discharging could not be completely decomposed during the following charging, meaning that deposits remained and accumulated inside the cathode at each cycle. The discharge capacity of o-CG was maintained at the set value for only 4 cycles. Irreversible capacities were observed from the 2nd cycle, indicating that the cyclability of o-CG was lower than that of p-CG, even though the overpotential required for charging o-CG was lower than that for p-CG. It has been reported that OCFGs existing on the surface of carbon materials promote side reactions during charging and discharging, such as the decomposition of the electrolyte[10]. Therefore, the obtained results suggest that the OCFGs in o-CG also promoted such side reactions.

On the other hand, the discharge capacities of o-300°C-CG and o-700°C-CG were maintained at the set value for 26 cycles and 22 cycles, respectively, and their charge capacities were maintained at the set value for up to 8 cycles and 11 cycles, respectively. These cycle numbers were significantly larger than those of p-CG and o-CG. Considering that the total numbers of OCFGs in o-CG and o-300°C-CG were close, these results suggest that not only the amounts of but also the type of OCFG significantly influences cycle

performance. As TPD analysis showed an obvious difference in the number of carboxyl groups existing within o-CG and within o-300°C-CG, carboxyl groups are thought to accelerate undesired side reactions. While the cyclability of o-700°C-CG was also improved by the removal of carboxylic groups, that of o-300°C-CG was slightly better. This can be explained by the reduction of Li_2O_2 deposition inside its mesopores caused by the removal of various OCFGs, such as carboxyl, lactone, and anhydride groups. In conclusion, the reason why o-300°C-CG showed the highest cycle performance was that its surface properties, where the number of OCFG was increased, and the carboxy group was selectively removed, reduced the overpotential required for charging while avoiding undesired side reactions.

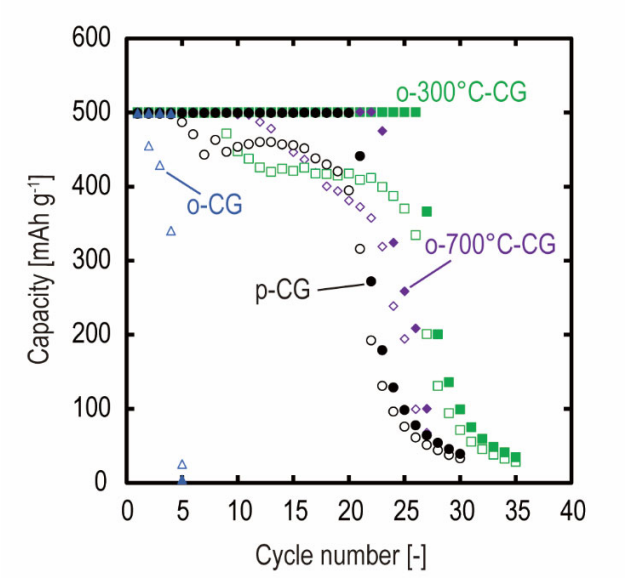

Figure12 Capacities of the surface modified CGs measured by discharge-charge cycle tests.The maximum discharge-charge capacity was set to 500 mAh g^{-1}. Filled and empty symbols represent discharge and charge capacities, respectively. The measurements were

conducted using coin-type cells.

4. Conclusion

In this study, it was demonstrated that the surface properties of carbon materials significantly influence the performance of it when used as the cathode material of Li-air batteries. The investigation, where CGs were used as a model porous carbon material, revealed that OCFGs existing at graphene edges in the material promote the deposition of Li_2O_2 inside its mesopores which leads to the reduction in the overpotential required for charging. In addition, edge H and carboxyl groups did not show a significant effect on the formation of Li_2O_2 inside mesopores. On the other hand, it was revealed that the effective functional groups which induce Li_2O_2 deposition inside mesopores were either anhydride, lactone, or phenol/ether. The OCFGs also promoted side reactions, which reduce cycle performance. This problem could be improved by simple heat treatment at 300°C in an inert atmosphere. As high-sensitivity TPD analysis revealed that this treatment selectively removed carboxyl groups, it is suggested that carboxyl groups on the carbon surface promote side reactions which lead to the deterioration of cathode performance. Therefore, it can be concluded that a trade-off relationship between charge overpotential reduction and side reaction suppression can be avoided by modifying both the number and types of OCFGs on the carbon surface. This study demonstrated the critical role of OCFGs in the carbon cathode during the cycling of LABs. The obtained knowledge can be utilized for developing a high-performance cathode of LABs.

Supporting information

Lithium air battery cells, peak separation of TPD analysis, XRD analysis of discharged CG electrodes after discharged, discharge-charge curves using different types of cells, influence of the particle size of CGs, discharge-charge curves of the cycle tests.

AUTHOR INFORMATION

Corresponding Authors

*E-mail: iwamura@eng.hokudai.ac.jp

*Phone: +81-11-706-6592

*E-mail: smukai@eng.hokudai.ac.jp

*Phone: +81-11-706-6590

Author Contributions

The manuscript was written through contributions of all authors. All authors have given approval to the final version of the manuscript.

ACKNOWLEDGMENT

This study was partly supported by JST ALCA-SPRING Grant Number JPMJAL1301, Japan. The samples were prepared with kind supports from Local Independent Administrative Agency Hokkaido Research Organization. They were analyzed partly by using the apparatus at Laboratory of Nano-Micro Material Analysis, Joint-use facilities, Hokkaido University.

ABBREVIATIONS

LAB, lithium-air battery; OCFG, oxygen-containing functional group; CG, carbon gel; TPD, temperature programmed desorption; CP, carbon paper; PVDF, polyvinylidene difluoride; NMP, N-methyl-2-pyrrolidone; DH, Dollimore-Heal; XRD, X-ray diffraction; TEGDME, tetraethylene glycol dimethyl ether; FE-SEM, field emission scanning electron microscope; FWHM, full width at half maximum.

References

(1) Dunn, B.; Kamath, H.; Tarascon, J. M. Electrical Energy Storage for the Grid: A Battery of Choices. *Science* **2011**, *334*, 928-935.

(2) Kang, S. J.; Mori, T.; Narizuka, S.; Wilcke, W.; Kim, H. C. Deactivation of Carbon Electrode for Elimination of Carbon Dioxide Evolution from Rechargeable Lithium-Oxygen Cells. *Nat. Commun.* **2014**, *5*.

(3) Ma, Z.; Yuan, X. X.; Li, L.; Ma, Z. F.; Wilkinson, D. P.; Zhang, L.; Zhang, J. J. A Review of Cathode Materials and Structures for Rechargeable Lithium-Air Batteries. *Energy Environ. Sci.* **2015**, *8*, 2144-2198.

(4) Ding, N.; Chien, S. W.; Hor, T. S. A.; Lum, R.; Zong, Y.; Liu, Z. L. Influence of Carbon Pore Size on the Discharge Capacity of Li-O_2 Batteries. *J. Mater. Chem. A* **2014**, *2*, 12433-12441.

(5) Sakai, K.; Iwamura, S.; Mukai, S. R. Influence of the Porous Structure of the Cathode on the Discharge Capacity of Lithium-Air Batteries. *J. Electrochem. Soc.* **2017**, *164*, A3075-A3080.

(6) Iwamura, S.; Fujita, K.; Nagaishi, S.; Sakai, K.; Mukai, S. R. Effect of Heat-Treatment Temperature of Carbon Gels on Cathode Performance of Lithium-Air Batteries. *J. Chem. Eng. Jpn.* **2021**, *54*, 213-218.

(7) Wang, F.; Xu, Y.-H.; Luo, Z.-K.; Pang, Y.; Wu, Q.-X.; Liang, C.-S.; Chen, J.; Liu, D.; Zhang, X.-h. A Dual Pore Carbon Aerogel Based Air Cathode for a Highly Rechargeable Lithium-Air Battery. *J. Power Sources* **2014**, *272*, 1061-1071.

(8) Lin, C.; Ritter, J. A. Effect of Synthesis Ph on the Structure of Carbon Xerogels. *Carbon* **1997**, *35*, 1271-1278.

(9) Belova, A. I.; Kwabi, D. G.; Yashina, L. V.; Shoo-Horn, Y.; Itkis, D. M. Mechanism of Oxygen Reduction in Aprotic Li-Air Batteries: The Role of Carbon Electrode Surface Structure. *J. Phys. Chem. C* **2017**, *121*, 1569-1577.

(10) Ottakam Thotiyl, M. M.; Freunberger, S. A.; Peng, Z.; Bruce, P. G. The Carbon Electrode in Nonaqueous Li–O_2 Cells. *J. Am. Chem. Soc.* **2013**, *135*, 494-500.

(11) Wong, R. A.; Dutta, A.; Yang, C. Z.; Yamanaka, K.; Ohta, T.; Nakao, A.; Waki, K.; Byon, H. R. Structurally Tuning Li_2o_2 by Controlling the Surface Properties of Carbon Electrodes: Implications for Li-O_2 Batteries. *Chem. Mater.* **2016**, *28*, 8006-8015.

(12) Dutta, A.; Ito, K.; Nomura, A.; Kubo, Y. Quantitative Delineation of the Low Energy Decomposition Pathway for Lithium Peroxide in Lithium-Oxygen Battery. *Adv. Sci.* **2020**, *7*.

(13) Xiao, J.; Mei, D.; Li, X.; Xu, W.; Wang, D.; Graff, G. L.; Bennett, W. D.; Nie, Z.; Saraf, L. V.; Aksay, I. A.; et al. Hierarchically Porous Graphene as a Lithium–Air Battery Electrode. *Nano Lett.* **2011**, *11*, 5071-5078.

(14) Laine, N. R.; Vastola, F. J.; Walker, P. L. The Importance of Active Surface Area in the

Carbon-Oxygen Reaction. *J Phys Chem* **1963**, *67*, 2030-2034.

(15) Yuan, W. J.; Zhou, Y.; Li, Y. R.; Li, C.; Peng, H. L.; Zhang, J.; Liu, Z. F.; Dai, L. M.; Shi, G. Q. The Edge- and Basal-Plane-Specific Electrochemistry of a Single-Layer Graphene Sheet. *Sci. Rep.* **2013**, *3*.

(16) Tran, V. V.; Nguyen, D. D.; Hofmann, M.; Hsieh, Y.-P.; Kan, H.-C.; Hsu, C.-C. Edge-Rich Interconnected Graphene Mesh Electrode with High Electrochemical Reactivity Applicable for Glucose Detection. *Nanomaterials* **2021**, *11*.

(17) Zhou, J. H.; Sui, Z. J.; Zhu, J.; Li, P.; De, C.; Dai, Y. C.; Yuan, W. K. Characterization of Surface Oxygen Complexes on Carbon Nanofibers by Tpd, Xps and Ft-Ir. *Carbon* **2007**, *45*, 785-796.

(18) Figueiredo, J. L.; Pereira, M. F. R.; Freitas, M. M. A.; Órfão, J. J. M. Modification of the Surface Chemistry of Activated Carbons. *Carbon* **1999**, *37*, 1379-1389.

(19) Bleda-Martínez, M. J.; Lozano-Castelló, D.; Morallón, E.; Cazorla-Amorós, D.; Linares-Solano, A. Chemical and Electrochemical Characterization of Porous Carbon Materials. *Carbon* **2006**, *44*, 2642-2651.

(20) Li, N.; Ma, X.; Zha, Q.; Kim, K.; Chen, Y.; Song, C. Maximizing the Number of Oxygen-Containing Functional Groups on Activated Carbon by Using Ammonium Persulfate and Improving the Temperature-Programmed Desorption Characterization of Carbon Surface Chemistry. *Carbon* **2011**, *49*, 5002-5013.

(21) Zielke, U.; Hüttinger, K. J.; Hoffman, W. P. Surface-Oxidized Carbon Fibers: I. Surface Structure and Chemistry. *Carbon* **1996**, *34*, 983-998.

(22) de la Puente, G.; Pis, J. J.; Menéndez, J. A.; Grange, P. Thermal Stability of

Oxygenated Functions in Activated Carbons. *J. Anal. Appl. Pyrolysis* **1997**, *43*, 125-138.

(23) Ishii, T.; Ozaki, J.-i. Understanding the Chemical Structure of Carbon Edge Sites by Using Deuterium-Labeled Temperature-Programmed Desorption Technique. *Carbon* **2020**, *161*, 343-349.

(24) Ishii, T.; Kashihara, S.; Hoshikawa, Y.; Ozaki, J.-i.; Kannari, N.; Takai, K.; Enoki, T.; Kyotani, T. A Quantitative Analysis of Carbon Edge Sites and an Estimation of Graphene Sheet Size in High-Temperature Treated, Non-Porous Carbons. *Carbon* **2014**, *80*, 135-145.

(25) Kyotani, T.; Ozaki, J.-i.; Ishii, T. What Can We Learn by Analyzing the Edge Sites of Carbon Materials? *Carbon Reports* **2022**, *1*, 188-205.

(26) Ishii, T.; Ozaki, J.-i. Estimation of the Spatial Distribution of Carbon Edge Sites in a Carbon Structure Using H_2 Desorption Kinetics in Temperature Programmed Desorption. *Carbon* **2022**, *196*, 1054-1062.

(27) Tang, R.; Taguchi, K.; Nishihara, H.; Ishii, T.; Morallon, E.; Cazorla-Amoros, D.; Asada, T.; Kobayashi, N.; Muramatsu, Y.; Kyotani, T. Insight into the Origin of Carbon Corrosion in Positive Electrodes of Supercapacitors. *J. Mater. Chem. A* **2019**, *7*, 7480-7488.

(28) Tang, R.; Yamamoto, M.; Nomura, K.; Morallón, E.; Cazorla-Amorós, D.; Nishihara, H.; Kyotani, T. Effect of Carbon Surface on Degradation of Supercapacitors in a Negative Potential Range. *J. Power Sources* **2020**, *457*, 228042.

(29) Choi, G. B.; Hong, S.; Wee, J. H.; Kim, D. W.; Seo, T. H.; Nomura, K.; Nishihara, H.; Kim, Y. A. Quantifying Carbon Edge Sites on Depressing Hydrogen Evolution Reaction Activity. *Nano Lett.* **2020**, *20*, 5885-5892.

(30) Nomura, K.; Nishihara, H.; Kobayashi, N.; Asada, T.; Kyotani, T. 4.4 V

Supercapacitors Based on Super-Stable Mesoporous Carbon Sheet Made of Edge-Free Graphene Walls. *Energy Environ. Sci.* **2019**, *12*, 1542-1549.

(31) Zaini, M. A. A.; Yoshida, S.; Mori, T.; Mukai, S. R. Preliminary Evaluation of Resorcinol-Formaldehyde Carbon Gels for Water Pollutants Removal. *Acta Chim. Slovaca* **2017**, *10*, 54-60.

(32) Ma, S. B.; Lee, D. J.; Roev, V.; Im, D.; Doo, S.-G. Effect of Porosity on Electrochemical Properties of Carbon Materials as Cathode For lithium-Oxygen Battery. *J. Power Sources* **2013**, *244*, 494-498.

(33) Liu, L. M.; Tan, S. L.; Horikawa, T.; Do, D. D.; Nicholson, D.; Liu, J. J. Water Adsorption on Carbon - a Review. *Adv. Colloid Interface Sci.* **2017**, *250*, 64-78.

(34) Nishioka, K.; Morimoto, K.; Kusumoto, T.; Harada, T.; Hase, Y.; Kamiya, K.; Nakanishi, S. Expansion of the Potential Region for Sustained Discharge of Non-Aqueous Li-O_2 Batteries Using an Oxygen-Enriched Carbon Cathode. *Chem. Lett.* **2019**, *48*, 562-565.

(35) Younesi, S. R.; Urbonaite, S.; Björefors, F.; Edström, K. Influence of the Cathode Porosity on the Discharge Performance of the Lithium–Oxygen Battery. *J. Power Sources* **2011**, *196*, 9835-9838.

(36) Matsuda, S.; Yamaguchi, S.; Yasukawa, E.; Asahina, H.; Kakuta, H.; Otani, H.; Kimura, S.; Kameda, T.; Takayanagi, Y.; Tajika, A.; et al. Effect of Electrolyte Filling Technology on the Performance of Porous Carbon Electrode-Based Lithium-Oxygen Batteries. *ACS Appl. Energy Mater.* **2021**, *4*, 2563-2569.

TOC Graphic

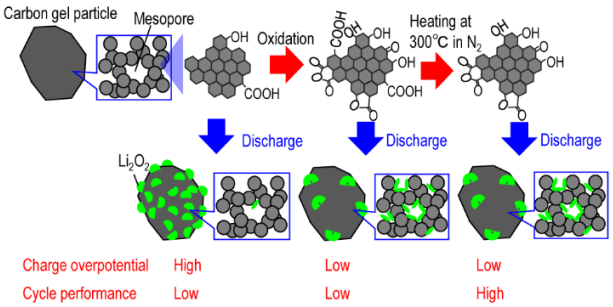
Carbon gel particle
Mesopore
OH
COOH
Oxidation
Heating at
300°C in N2
Discharge
Discharge
Discharge
Li2O2
Charge overpotential
Cycle performance
High
Low
Low
Low
Low
High